

Autofluorescence and diffuse reflectance spectroscopy of oral epithelial tissue using a depth-sensitive fiber-optic probe

Richard A. Schwarz,^{1,*} Wen Gao,¹ Dania Daye,¹ Michelle D. Williams,²
Rebecca Richards-Kortum,¹ and Ann M. Gillenwater³

¹Department of Bioengineering MS 142, Rice University, 6100 Main Street, Keck Hall Suite 116, Houston, Texas 77005, USA

²Department of Pathology, The University of Texas M.D. Anderson Cancer Center, 1515 Holcombe Boulevard, Houston, Texas 77030, USA

³Department of Head and Neck Surgery, The University of Texas M.D. Anderson Cancer Center, 1515 Holcombe Boulevard, Houston, Texas 77030, USA

*Corresponding author: schwarzr@rice.edu

Received 20 August 2007; revised 13 December 2007; accepted 27 December 2007;
posted 7 January 2008 (Doc. ID 86503); published 20 February 2008

Optical spectroscopy can provide useful diagnostic information about the morphological and biochemical changes related to the progression of precancer in epithelial tissue. As precancerous lesions develop, the optical properties of both the superficial epithelium and underlying stroma are altered; measuring spectral data as a function of depth has the potential to improve diagnostic performance. We describe a clinical spectroscopy system with a depth-sensitive, ball lens coupled fiber-optic probe for noninvasive *in vivo* measurement of oral autofluorescence and diffuse reflectance spectra. We report results of spectroscopic measurements from oral sites in normal volunteers and in patients with neoplastic lesions of the oral mucosa; results indicate that the addition of depth selectivity can enhance the detection of optical changes associated with precancer. © 2008 Optical Society of America

OCIS codes: 170.6510, 170.3890, 060.2310.

1. Introduction

Cancers of the oral cavity and oropharynx are annually responsible for more than 7500 deaths in the United States and an estimated 127,000 deaths worldwide [1,2]. In the United States, patients diagnosed with oral or oropharyngeal cancer have a five-year survival rate of 59% relative to people of the same age group, gender, and ethnicity who do not have cancer [1]. This survival rate has changed little over the past 30 years, in part because most patients present with disease that is already at an advanced stage [3]. Better methods for early detection and diagnosis of oral cancer are needed to improve patient outcomes.

Standard clinical practice for diagnosis of oral cancer consists of visual inspection followed by invasive biopsy and histologic examination of any sites that appear abnormal. However, visual identification of the more subtle changes associated with early lesions can be difficult even for experienced clinicians. Most clinically apparent oral lesions, such as candidiasis and aphthous ulcers, are benign; other lesions, such as leukoplakia, are associated with a risk of malignant progression that is difficult to judge by appearance alone. Furthermore, especially in patients with chronic exposure to carcinogens, histologic and genetic damage may exist even in areas in which the mucosa appears normal [4].

A variety of technologies designed to aid the clinician in detecting and diagnosing oral neoplasia are under development [5]. Optical spectroscopy is a

noninvasive technique whose potential to facilitate diagnosis of oral lesions has been demonstrated by a number of groups [6–12]. Loss of autofluorescence in the blue–green region of the spectrum is thought to be diagnostically significant, and according to recent reports may be associated with subclinical genetic alterations in the cancer risk field [4]; but the nature of this association has not been explained.

The development and progression of oral neoplasia has been reported to be associated with a variety of changes in tissue optical properties, including changes in the concentration of fluorophores such as reduced nicotinamide adenine dinucleotide (NADH), flavin adenine dinucleotide (FAD), and keratin; changes in fluorescent collagen crosslinks in the underlying stroma; changes in tissue scattering due to alterations in cell morphology; changes in hemoglobin absorption due to increased microvascularization; and changes in the thickness of the epithelial layer [13–16]. While fluorescence microscopy studies of excised fresh tissue provide insight into the spatial dependence of optical property changes that accompany neoplasia [17,18], it is more difficult to interpret spectroscopic measurements made from intact tissue. The precise mechanisms underlying the observed changes in tissue autofluorescence are not well understood [19]. As neoplastic lesions develop, the morphological and biochemical properties of both the epithelium and stroma change, often in very different ways. If tissue spectra are acquired *in vivo* using an optical system that simply integrates optical signals arising from different depths, then optical changes arising in the epithelium and stroma may produce dissimilar or even opposing contributions to spectra measured from intact tissue. While a variety of mathematical models have been developed to analyze measured tissue spectra and deconvolve optical changes that occur in the epithelium and stroma, most of these models include many variables that describe multiple competing effects, and typically require prior knowledge or assumptions regarding some input parameters such as the depth-dependent distribution of specific chromophores in the tissue [20–23]. Results generated by these models, such as concentrations of fluorophores in tissue *in vivo*, are difficult to validate.

These issues must be addressed as optical spectroscopy and spectroscopic imaging move increasingly into clinical use for detection and diagnosis of oral lesions. The use of a depth-sensitive spectroscopy device that is capable of selectively targeting the epithelium or stroma may provide a means of overcoming some of these limitations. The ability to disentangle the changes in optical properties that arise in the epithelium and stroma may prove useful in improving the diagnostic ability of optical spectroscopy, particularly for the detection of early neoplastic lesions that originate in the epithelium.

A number of probe designs and techniques intended to target specific sampling regions in tissue have been reported [24]. Oblique-incidence illumina-

tion and/or collection geometries using angled fibers have been used to target superficial tissue regions [25–27]. Variations in fiber size, illumination-collection fiber separation, and probe-sample spacing have been shown to influence sensitivity to different fluorophore layers in turbid media [28]. Differential path-length spectroscopy has been demonstrated as a technique for preferential detection of photons scattered from shallow depths [29].

We have previously described the design of a ball lens coupled fiber-optic probe for depth-resolved spectroscopy and validated its performance in tissue phantoms [30]. In this paper we present a clinical spectroscopy system based on this depth-sensitive probe, designed for noninvasive *in vivo* measurement of autofluorescence and diffuse reflectance spectra of oral mucosa. We present representative spectral measurements of oral sites in healthy normal volunteers and in patients with neoplastic lesions of the oral mucosa. Results indicate that the addition of depth selectivity can enhance the detection of optical changes associated with precancer.

2. Materials and Methods

A. Instrumentation

A schematic and photograph of the clinical spectroscopy system are shown in Fig. 1. The device is housed in a mobile cart 0.6 m × 0.8 m × 1.3 m in size. The light source is a 75 W xenon arc lamp (Photon Technology International, Birmingham, N.J.). Two filter wheels (Sutter Instrument Company, Novato, Calif.) containing bandpass filters (Chroma Technology Corporation, Rockingham, Vt.) allow selection of twelve different excitation wavelengths between 300 and 470 nm for fluorescence measurements, or broadband light at various illumination levels for reflectance measurements. The full-width at half-maximum transmission bandwidth for the fluorescence excitation filters is 7 nm. Exposure time is controlled by a shutter (Vincent Associates, Rochester, N.Y.) located in the illumination pathway. Excitation light is coupled into one of four illumination channels in the fiber-optic probe, selected by means of a motorized translation stage (Parker Hannifin Corporation, Cleveland, Ohio). Illumination power is measured using two power meters (Newport Corporation, Irvine, Calif.). One power meter is used for direct measurements of probe output during system calibration; the other is permanently coupled to sampling fibers in the probe to monitor the illumination power and exposure time during the tissue measurement.

Figure 2 shows a photograph of the fiber optic probe and a diagram of the arrangement of illumination and detection fibers at its distal end. The design concept of the ball lens coupled probe has been previously described [30]. The clinical probe described here contains four channels that are identified in terms of their depth response characteristics: a “shallow” channel, a “medium” depth channel, and two

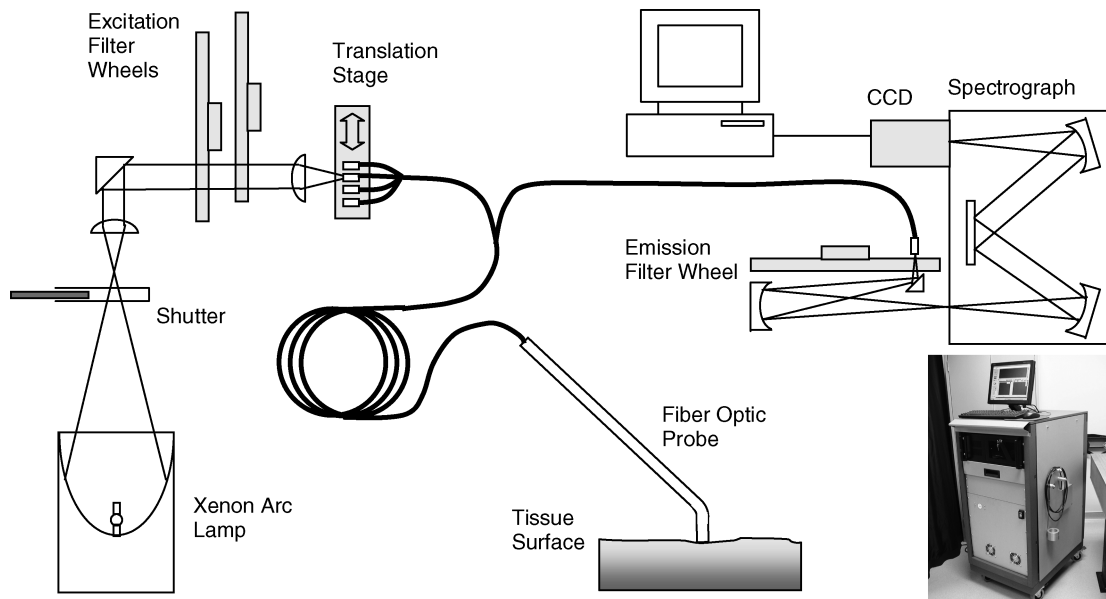


Fig. 1. Diagram and photograph of the clinical spectroscopy system.

“deep” channels. In the shallow and medium channels, light is delivered to the tissue and collected through a 2 mm diameter sapphire ball lens. The ball lens is mounted in a stainless steel outer disk at the distal tip of the probe. The fibers for the shallow and medium channels terminate in a stainless steel inner disk, which is located just inside the probe tip and is separated from the ball lens by a 0.50 mm air gap. The shallow channel contains 14 illumination fibers arranged in a circle of radius 0.72 mm. The medium channel contains six illumination fibers arranged in a concentric circle of radius 0.36 mm. A single collection fiber, serving both the shallow and medium channels, is located at the center of both circles. The shallow and medium channels collect signal preferentially from different depths beneath the same location on the tissue surface. The fibers for the two deep channels terminate in the outer disk adjacent to the ball lens, with one channel on each side of the ball lens. The two deep channels are identical to each other in design. Each contains two illumination fibers and one adjacent collection fiber, all in direct contact with the tissue. The deep channels interrogate tissue sites located approximately 1.4 mm on either side of the site interrogated by the shallow and medium channels. All optical fibers (Polymicro Technologies, Phoenix, Ariz.) have a 200 μm core diameter and a numerical aperture of 0.22.

Upon illumination of the tissue, detected light (autofluorescence or diffuse reflectance) returns through the collection channels of the probe and emerges from fibers arranged in a vertical stack. The collected light passes through a filter wheel containing longpass filters and is directed onto the entrance slit of an imaging spectrograph (Horiba Jobin Yvon, Longjumeau, France). A TE-cooled CCD camera (Andor Technology, Belfast, Northern Ire-

land) located at the exit port of the spectrograph collects an image that contains the spectrum of collected light from each fiber in the stack.

All system instrumentation is controlled by Labview software (National Instruments Corporation, Austin, Tex.). The measurement sequence is fully automated and a single measurement takes approximately 90 s. During a measurement the instrument collects 52 individual spectra: fluorescence spectra at 12 different excitation wavelengths in the range 300–470 nm and one broadband diffuse reflectance spectrum, through each of the four depth-selective probe channels. Background spectra, with the illumination source blocked, are also collected during the measurement.

B. Measurement and Modeling of Probe Depth Response

To measure the depth response of the clinical probe, a single side of a microscope slide was coated with a thin ($< 15 \mu\text{m}$) uniform layer of green fluorescent paint for use as a test target. The response of each probe channel to the fluorescent target was measured as a function of distance from the probe tip to the target. This experiment was first performed in air and was then repeated with the probe and target fully immersed in water, to better simulate the refractive index change that would be encountered when the probe is in contact with tissue.

The measurements described above provide only an approximation of the actual depth response of the probe in tissue, since tissue is a highly scattering medium compared to air or water. Monte Carlo simulations were performed to evaluate the effect of scattering on depth response. A previously reported Monte Carlo model [31] was modified to simulate the clinical ball lens probe geometry and the experimental conditions corresponding to the depth re-

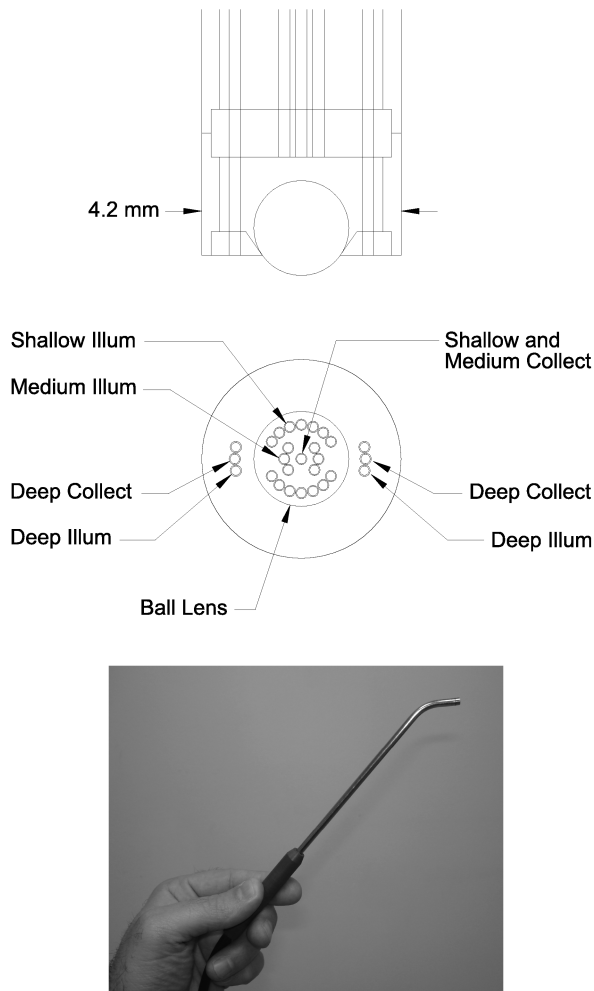


Fig. 2. Diagram and photograph of the clinical ball lens coupled fiber-optic probe.

sponse measurement using a fluorescent target immersed in water. Simulations were performed with a range of scattering coefficients assigned to the medium: nonscattering ($\mu_s = 0 \text{ cm}^{-1}$), moderate scattering ($\mu_s = 47 \text{ cm}^{-1}$), and high scattering ($\mu_s = 224 \text{ cm}^{-1}$). Results of the simulations were compared to measured data.

C. *In Vivo* Spectral Measurements

Protocols were approved by the Institutional Review Boards at the University of Texas M.D. Anderson Cancer Center (MDACC) and Rice University. Sites within the oral cavity of patients with oral lesions and normal volunteers were measured using the device. For each patient, spectroscopic measurements were acquired from several sites, including clinically suspicious lesions selected by the clinician and at least one contralateral, clinically normal appearing site. At each measurement site, the probe was placed in gentle contact with the mucosal surface of the tissue for the duration of the spectroscopic measurement. The procedure was performed in a darkened room to minimize variability and artifact from exposure to ambient light. Wavelength calibration, power

calibration, and standards measurements were performed immediately before or after the patient measurements. After the spectroscopic measurements were completed, biopsies were collected from the corresponding tissue sites for histologic examination, subject to prior patient consent and the discretion of the clinician. Histologic results were reviewed by a study pathologist. For normal volunteers, the same procedure was followed for spectroscopic measurements; clinical appearance of measured sites was noted but no biopsies were performed.

D. Calibration and Data Processing

Wavelength calibration was performed using a mercury-argon calibration lamp (Ocean Optics, Dunedin, Fla.). Standards measured daily included two positive fluorescence standards (Rhodamine B in ethylene glycol, 2 mg/L and 8 g/L); two negative fluorescence standards (frosted surface of a quartz cuvette and deionized ultrafiltered water); and a positive reflectance standard (Teflon). The spectrum of a calibrated tungsten halogen light source (Ocean Optics) was obtained and used to correct measured spectra for nonuniform spectral variations in the throughput of the detection system.

Measured spectra were processed using Matlab (The MathWorks, Natick, Mass.). A median filter was first applied to remove single-pixel outliers and a Savitzky-Golay filter was used to remove high-frequency noise. Each tissue fluorescence measurement was normalized by the illumination energy delivered to the tissue and corrected for variations in the spectral transmission characteristics of the detection system. Diffuse reflectance spectra of tissue were divided by the corresponding diffuse reflectance spectra of the Teflon reflectance standard to obtain the ratio of tissue reflectance to this standard.

3. Results

A. Probe Depth Response Data

The measured depth response of the shallow channel, medium channel, and a representative deep channel of the clinical ball lens coupled probe are shown in Figs. 3(a) and 3(b). The normalized fluorescence intensity is plotted as a function of distance from the probe tip to the fluorescent target. The probe tip is formed by the distal surface of the ball lens, which extends 0.43 mm beyond the surface of the outer disk where the deep channel fibers terminate. Therefore when the probe tip is in contact with a noncompliant surface such as the microscope slide used in this measurement, the shallow and medium channels are in direct contact with the target but the deep channels are recessed by 0.43 mm. The data shown were measured using an excitation wavelength of 400 nm; measurements obtained at other excitation wavelengths were similar. Figure 3(a) shows results obtained with the probe and target in air. In the shallow channel, the fluorescence intensity drops to 10% of its peak value within 320 μm of

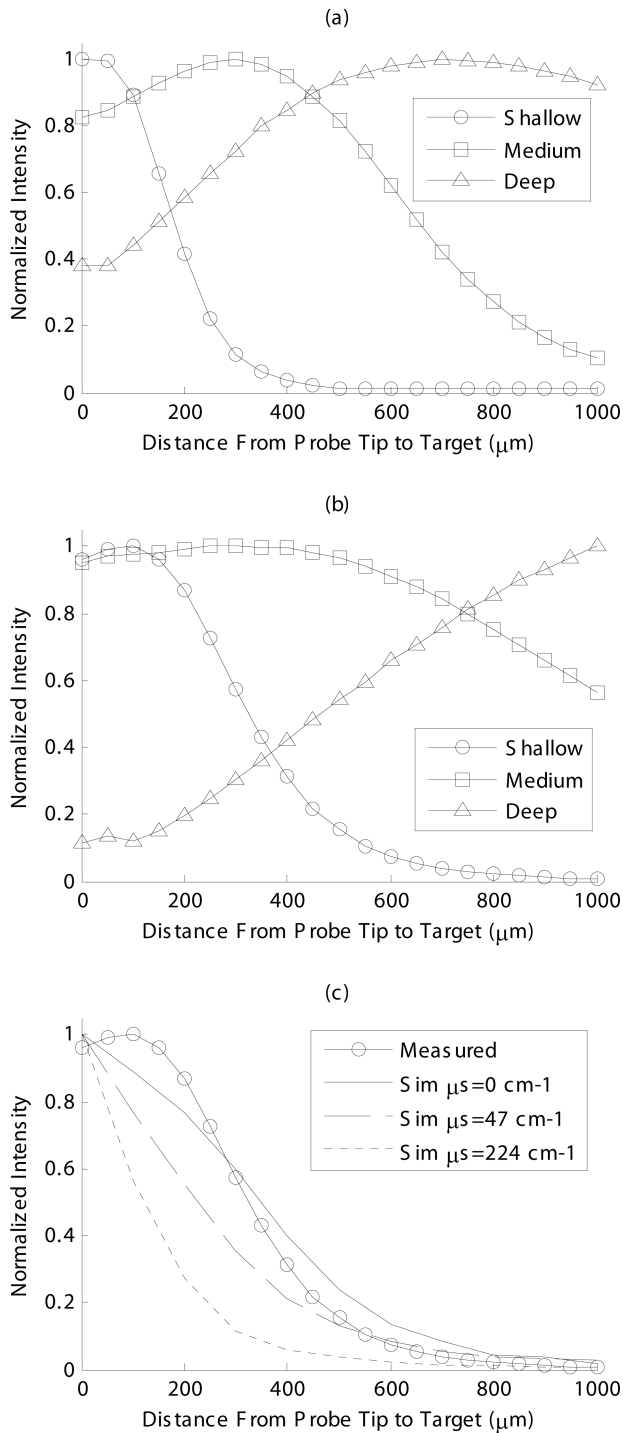


Fig. 3. Measured depth response of the probe and comparison with simulations: (a) measured depth response in air; (b) measured depth response in water; (c) measured depth response in water versus Monte Carlo simulated depth response for nonscattering, moderately scattering, and highly scattering media (shallow channel only).

the probe tip. Figure 3(b) shows the same measurement performed with both the probe and target immersed in water. In this case the depth response curve broadens and shifts slightly deeper due to the reduced refraction of illumination rays at the probe–water interface. This is a better indication

of the depth response that would be expected with the probe in contact with tissue. In water, the fluorescence intensity in the shallow channel drops to 10% of its peak value within 550 μm of the probe tip.

Figure 3(c) shows the measured depth response for the shallow channel in water compared to the Monte Carlo simulated depth response for the shallow channel. Monte Carlo results are shown for three different cases: a nonscattering medium ($\mu_s = 0 \text{ cm}^{-1}$), a moderately scattering medium ($\mu_s = 47 \text{ cm}^{-1}$), and a highly scattering medium ($\mu_s = 224 \text{ cm}^{-1}$). The Monte Carlo result in the nonscattering case is roughly comparable to the measured depth response in water. The simulations indicate that as scattering increases the depth response is confined to shallower depths. This is consistent with results reported by Pfefer *et al.* from a Monte Carlo simulation of a similar oblique-incidence illumination geometry, in which increasing attenuation was found to decrease the probing depth [27]. We conclude from these modeling results that the measured depth response in water provides a rough approximation of the depth response in tissue but tends to overestimate the actual probing depth.

B. *In Vivo* Spectral Data

Using this system, we obtained spectroscopic measurements from 188 sites in 39 patients with lesions of the oral mucosa and from 140 sites in 32 normal volunteers. Figure 4 shows a representative example of spectra collected from a single site on the lateral tongue in a normal volunteer. The data shown are fluorescence emission spectra collected at three excitation wavelengths (330, 350, and 400 nm) and reflectance spectra collected using white light illumination. Data from the shallow channel and a deep channel of the probe are shown for comparison. The spectra shown represent eight of the 52 spectra that are collected in a given spectroscopic measurement. The reflectance spectra and several of the fluorescence spectra shown exhibit a valley at 420 nm, which is attributed to the presence of the absorber hemoglobin that has a peak absorption at this location. Fluorescence and reflectance spectra acquired through the deep channel of the probe show a substantially increased contribution of hemoglobin absorption than do measurements made through the shallow channel. Since blood vessels are expected to be present in the stroma but not in the epithelium, this is a good indication that the fraction of signal collected from the epithelium is greater for the shallow channel than for the deep channels.

Figure 5 shows representative fluorescence emission spectra collected from normal, dysplastic, and cancerous sites of the buccal mucosa in a single oral cancer patient at 350 nm excitation, using (a) the shallow channel and (b) a deep channel of the probe. Figures 5(c) and 5(d) show the same spectra normalized to their peak intensity values for comparison. Spectra measured using both the shallow and deep channels indicate progressively lower fluorescence

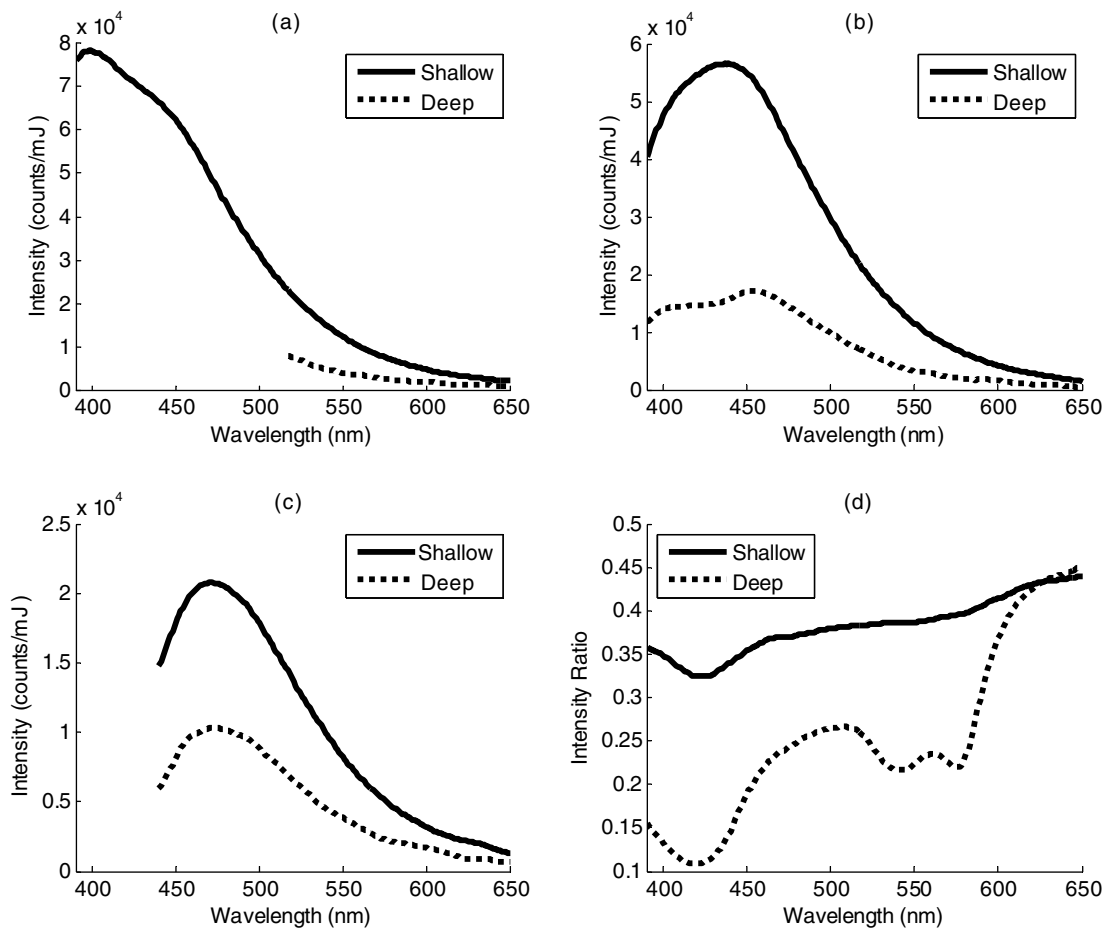


Fig. 4. Spectra measured from a single lateral tongue site in a normal volunteer using the shallow and deep channels of the probe: (a) fluorescence spectrum at 330 nm excitation; (b) fluorescence spectrum at 350 nm excitation; (c) fluorescence spectrum at 400 nm excitation; (d) diffuse reflectance spectrum under white light illumination. All spectra are shown on the same wavelength scale for comparison; the fluorescence spectrum at 400 nm excitation was collected with a 435 nm emission filter. The absorptions at 420, 540, and 580 nm in the deep channel reflectance spectrum are attributed to hemoglobin. The 420 nm hemoglobin absorption is evident in the reflectance spectra and also in several of the fluorescence spectra, particularly those collected using the deep channel.

intensity from the dysplastic and cancerous tissue sites compared to the normal site. The spectrum of the normal site collected through the deep channel shows a strong absorption at 420 nm that is absent in the corresponding shallow channel spectrum; again, this is consistent with the presence of hemoglobin in the stroma but not in the epithelium. In the shallow channel, it is interesting to note that there is a shift to longer peak wavelengths in the fluorescence spectra of the abnormal sites with respect to the normal site. Since the shallow channel enhances signal collection from the epithelium, this wavelength shift is consistent with increased relative contributions of NADH and FAD to the fluorescence spectra in the epithelial layer of the abnormal tissue sites [17,18].

Figure 6 shows representative fluorescence emission spectra collected from normal, dysplastic, and cancerous sites in the lateral tongue in a single oral cancer patient at 350 nm excitation, using (a) the shallow channel and (b) a deep channel of the probe. Figures 6(c) and 6(d) show the same spectra normalized to their peak intensity values for comparison.

The spectra show trends similar to those observed in Fig. 5. Lower fluorescence intensity is observed from the dysplastic and cancerous sites compared to the normal site in both the shallow channel and deep channel spectra. Hemoglobin absorption is more evident in the spectra measured through the deep channel. In the shallow channel there is a pronounced wavelength shift in the spectra of the abnormal sites compared to the spectrum of the normal site. In this case a wavelength shift is also apparent in the deep channel spectra.

4. Discussion

Previous reports have documented the potential of fluorescence and reflectance spectroscopy for noninvasive diagnosis of early oral cancer and precancer. However, to be effective clinically, diagnostic technologies need to have high specificity, as well as sensitivity, in order to avoid unnecessary patient interventions. Recent advances in the understanding of the alterations in tissue optical properties during carcinoma development have identified distinct dif-

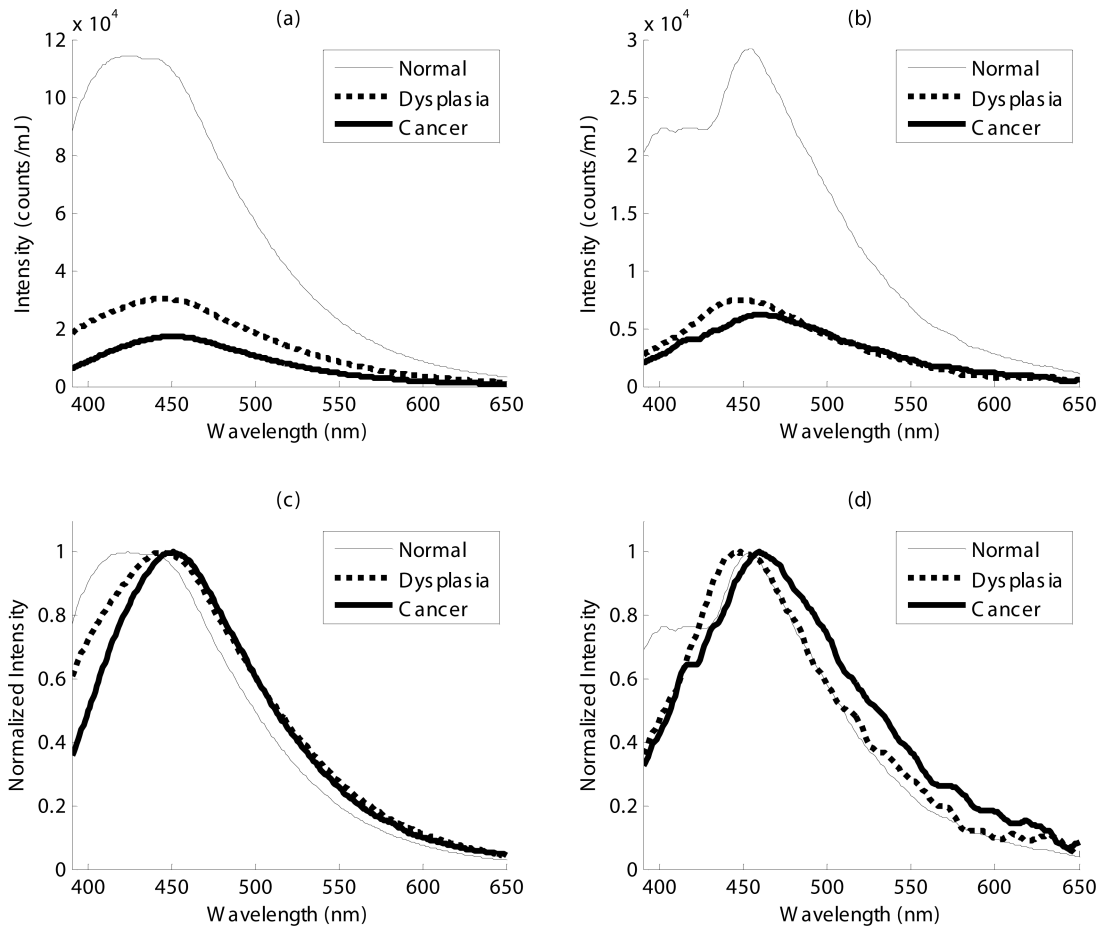


Fig. 5. Fluorescence spectra measured from three buccal sites in a single oral cancer patient at 350 nm excitation: (a) shallow channel, (b) deep channel, (c) shallow channel normalized to peak intensity value, and (d) deep channel normalized to peak intensity value. Histologic diagnoses of the three sites are, respectively, normal, moderate dysplasia, and well-differentiated invasive cancer.

ferences between the epithelium and the underlying stroma [17]. This suggests that separate interrogation of epithelial and stromal layers may improve the ability to distinguish dysplasia and carcinoma from normal mucosa and benign conditions.

The spectroscopy system described in this report allows *in vivo* measurements of oral fluorescence and diffuse reflectance spectra at different depths within the tissue. The depth response measurements shown in Fig. 3 indicate how well the depth-sensitive clinical probe performs. The measurements taken with the probe immersed in water, Fig. 3(b), provide an estimate of the depth sensitivity of the probe for tissue measurements, though the actual probing depth may be slightly shallower due to scattering in tissue. In the oral cavity the thickness of the epithelial layer is typically of the order of 300–500 μm , varying with the specific tissue type. Figure 3(b) indicates that the shallow channel is strongly weighted towards the epithelial layer (the first 300–500 μm), but does not completely exclude signal from the stroma. The degree to which the interrogated region is confined to the epithelium depends on the epithelial thickness and therefore on tissue type within the oral cavity. The medium

channel collects signal from a broad region that includes both epithelium and stroma, extending from the tissue surface to depths greater than 1 mm. The deep channels primarily interrogate the stroma but do include a small component of signal from the epithelium.

The most prominent general feature observed in our *in vivo* data collected to date is a progressive overall reduction in blue–green fluorescence intensity in dysplastic and cancerous tissue compared to normal tissue, as illustrated in Figs. 5(a), 5(b), 6(a), and 6(b). This trend is evident across a wide range of excitation wavelengths from 330 to 470 nm, though not at 300 or 310 nm excitation. The reduction in fluorescence intensity in dysplasia and carcinoma is observed in all oral tissue types measured and in all depth channels of the probe (shallow, medium, and deep), indicating that alterations in both epithelium and stroma are involved. We believe the most likely contributing factors to this reduction in fluorescence intensity are the breakdown of collagen crosslinks in the stroma, thickening of the epithelium, increased epithelial scattering, loss of keratin in the epithelium, and increased hemoglobin absorption associated with increased microvascular

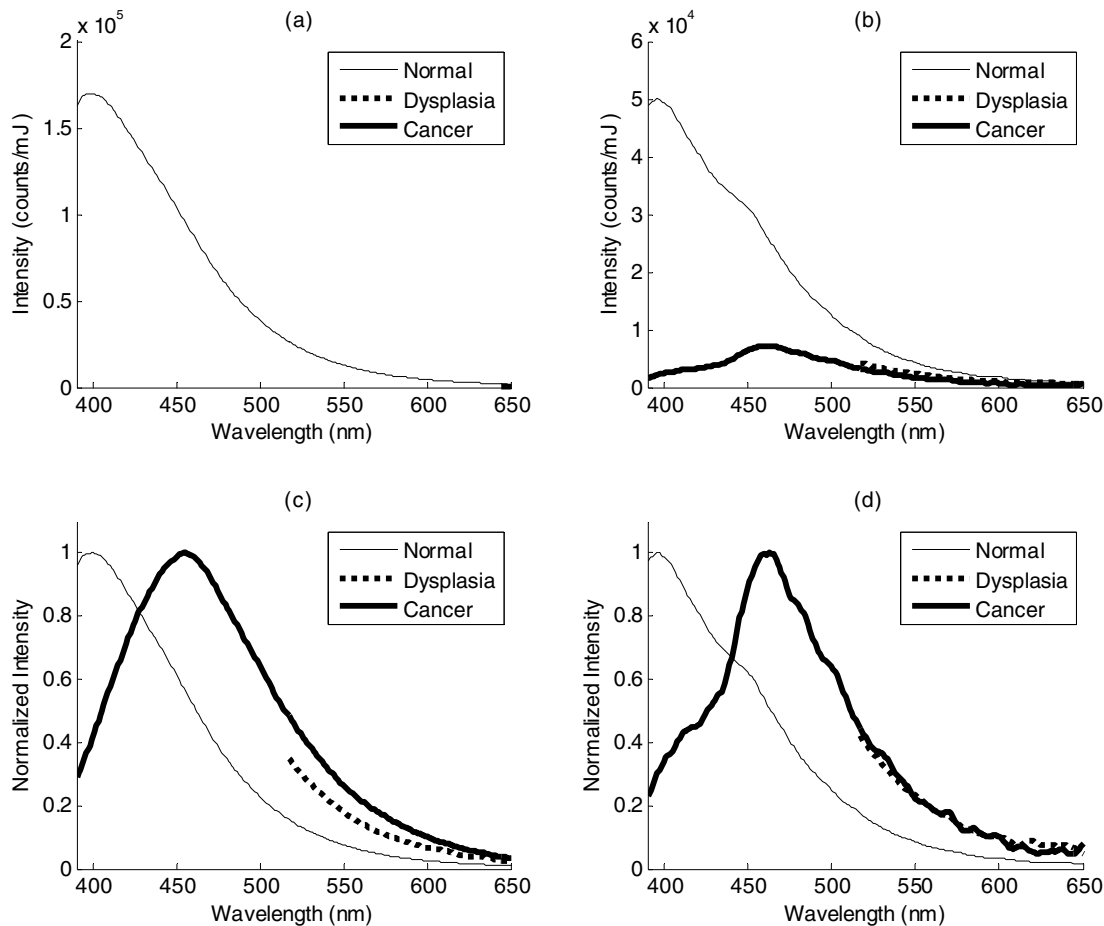


Fig. 6. Fluorescence spectra measured from three lateral tongue sites in a single oral cancer patient at 350 nm excitation: (a) shallow channel, (b) deep channel, (c) shallow channel normalized to peak intensity value, and (d) deep channel normalized to peak intensity value. Histologic diagnoses of the three sites are, respectively, normal, mild dysplasia, and moderately differentiated invasive cancer.

density throughout the epithelial–stromal region [16,32,33].

A second general feature observed in the data is a progressive shift of the blue–green fluorescence peak to longer wavelengths in dysplastic and cancerous tissue compared to normal tissue, as shown in Figs. 5(c) and 6(c). This trend also appears across a range of excitation wavelengths, most notably in the 330–390 nm range and somewhat less consistently in the 400–470 nm range. It is mostly seen in the shallow and medium channels, and less clearly observed in the deep channels; this may be because hemoglobin absorption distorts the shape of the normal spectra measured using the deep channels, as seen in Fig. 5(d), making the wavelength shift less readily apparent. The origin of the wavelength shift is not known but it may be associated with loss of fluorophores that emit at shorter wavelengths, such as keratin and collagen, and increased relative contributions to the fluorescence signal from NADH and FAD.

The reduction in blue–green fluorescence intensity and the associated wavelength shift that we observe in our data are consistent with results reported in the literature for *in vivo* oral measurements. In a pre-

vious study (without a ball lens coupled probe), our group found a reduction in blue–green fluorescence intensity and a wavelength shift in cancerous tissue compared to normal tissue, with excitation wavelengths of 365, 337, and 410 nm [14]. Badizadegan *et al.* reported a similar progressive reduction in fluorescence intensity and wavelength shift in dysplastic and cancerous oral tissue compared to normal tissue, with an excitation wavelength of 337 nm [9]. De Veld *et al.* found a progressive decrease in blue–green fluorescence intensity in dysplastic and tumor tissue compared to healthy tissue at 405 nm excitation, but also found a decrease in the fluorescence intensity of benign lesion sites compared to healthy tissue [10]. This raises the concern that this parameter may not provide sufficient specificity to distinguish dysplastic and cancerous lesions from benign lesions. Since inflammatory lesions predominantly affect the stroma, whereas dysplasia also produces alterations in the epithelium, spectral data separately derived from these layers may provide novel parameters to distinguish these clinical entities.

Our initial results indicate that the clinical ball lens coupled probe functions as designed and provides depth-sensitive *in vivo* spectral data. The shal-

low channel of the probe appears to minimize the effect of hemoglobin absorption on the fluorescence spectrum. It remains to be seen whether the removal of the hemoglobin absorption leads to significantly improved diagnostic performance; whether the probe can be used to identify different trends in fluorescence associated with fluorophores located in the epithelium and stroma; how diagnostic performance is affected by interpatient and inpatient variability; and whether benign and malignant lesions can be distinguished.

In summary, we have described a clinical spectroscopy system with a depth-sensitive fiber-optic probe for noninvasive *in vivo* measurement of oral sites in healthy subjects and in patients with lesions of the oral mucosa. Differences have been observed in intensity, peak emission wavelength, and shape of the fluorescence spectra of normal and abnormal tissue sites. Depth-sensitive spectral measurements have been successfully demonstrated *in vivo*. The ability to obtain spectra from different depths at a single measurement site, and to distinguish between epithelial and stromal spectral signatures, may improve the diagnostic capability of point probe optical spectroscopy systems.

The authors thank Adel K. El-Naggar for reviewing histopathology results, and Bimal Patel, Erica M. Smith, and Cristina Kurachi for performing *in vivo* measurements. The authors gratefully acknowledge support from National Cancer Institute grant R01CA095604.

References

1. L. A. G. Ries, D. Melbert, M. Krapcho, A. Mariotto, B. A. Miller, E. J. Feuer, L. Clegg, M. J. Horner, N. Howlader, M. P. Eisner, M. Reichman, and B. K. Edwards, eds., "SEER cancer statistics review, 1975–2004," National Cancer Institute, Bethesda, Md., based on November 2006 SEER data submission, posted to the SEER web site, 2007, http://seer.cancer.gov/csr/1975_2004/.
2. D. M. Parkin, F. Bray, J. Ferlay, and P. Pisani, "Global cancer statistics, 2002," *Ca-Cancer J. Clin.* **55**, 74–108 (2005).
3. B. W. Neville and T. A. Day, "Oral cancer and precancerous lesions," *Ca-Cancer J. Clin.* **52**, 195–215 (2002).
4. C. F. Poh, L. Zhang, D. W. Anderson, J. S. Durham, P. M. Williams, R. W. Priddy, K. W. Berean, S. Ng, O. L. Tseng, C. MacAulay, and M. P. Rosin, "Fluorescence visualization detection of field alterations in tumor margins of oral cancer patients," *Clin. Cancer Res.* **12**, 6716–6722 (2006).
5. A. Gillenwater, V. Papadimitrakopoulou, and R. Richards-Kortum, "Oral premalignancy: new methods of detection and treatment," *Curr. Oncol. Rep.* **8**, 146–154 (2006).
6. V. R. Kolli, H. E. Savage, T. J. Yao, and S. P. Schantz, "Native cellular fluorescence of neoplastic upper aerodigestive mucosa," *Arch. Otolaryngol. Head Neck Surg.* **121**, 1287–1292 (1995).
7. J. K. Dhingra, D. F. Perrault Jr., K. McMillan, E. E. Rebeiz, S. Kabani, R. Manoharan, I. Itzkan, M. S. Feld, and S. M. Shapshay, "Early diagnosis of upper aerodigestive tract cancer by autofluorescence," *Arch. Otolaryngol. Head Neck Surg.* **122**, 1181–1186 (1996).
8. C. S. Betz, M. Mehlmann, K. Rick, H. Stepp, G. Grevers, R. Baumgartner, and A. Leunig, "Autofluorescence imaging and spectroscopy of normal and malignant mucosa in patients with head and neck cancer," *Lasers Surg. Med.* **25**, 323–334 (1999).
9. K. Badizadegan, V. Backman, C. W. Boone, C. P. Crum, R. R. Dasari, I. Georgakoudi, K. Keefe, K. Munger, S. M. Shapshay, E. E. Sheets, and M. S. Feld, "Spectroscopic diagnosis and imaging of invisible pre-cancer," *Faraday Discuss.* **126**, 265–279 (2004).
10. D. C. G. de Veld, M. Skurichina, M. J. H. Witjes, R. P. W. Duin, H. J. C. M. Sterenberg, and J. L. N. Roodenburg, "Clinical study for classification of benign, dysplastic, and malignant oral lesions using autofluorescence spectroscopy," *J. Biomed. Opt.* **9**, 940–950 (2004).
11. D. C. G. de Veld, M. Skurichina, M. J. H. Witjes, R. P. W. Duin, H. J. C. M. Sterenberg, and J. L. N. Roodenburg, "Autofluorescence and diffuse reflectance spectroscopy for oral oncology," *Lasers Surg. Med.* **36**, 356–364 (2005).
12. S. K. Majumder, A. Gupta, S. Gupta, N. Ghosh, and P. K. Gupta, "Multi-class classification algorithm for optical diagnosis of oral cancer," *J. Photochem. Photobiol., B* **85**, 109–117 (2006).
13. A. Fryen, H. Glanz, W. Lohmann, T. Dreyer, and R. M. Bohle, "Significance of autofluorescence for the optical demarcation of field cancerisation in the upper aerodigestive tract," *Acta Otolaryngol. (Stockh.)* **117**, 316–319 (1997).
14. A. Gillenwater, R. Jacob, R. Ganeshappa, B. Kemp, A. K. El-Naggar, J. L. Palmer, G. Clayman, M. F. Mitchell, and R. R. Richards-Kortum, "Noninvasive diagnosis of oral neoplasia based on fluorescence spectroscopy and native tissue autofluorescence," *Arch. Otolaryngol. Head Neck Surg.* **124**, 1251–1258 (1998).
15. M. G. Müller, T. A. Valdez, I. Georgakoudi, V. Backman, C. Fuentes, S. Kabani, N. Laver, Z. Wang, C. W. Boone, R. R. Dasari, S. M. Shapshay, and M. S. Feld, "Spectroscopic detection and evaluation of morphologic and biochemical changes in early human oral carcinoma," *Cancer* **97**, 1681–1692 (2003).
16. P. M. Lane, T. G. P. Whitehead, H. Zeng, C. F. Poh, S. Ng, P. M. Williams, L. Zhang, M. P. Rosin, and C. E. MacAulay, "Simple device for the direct visualization of oral-cavity tissue fluorescence," *J. Biomed. Opt.* **11**, 024006 (2006).
17. I. Pavlova, K. Sokolov, R. Drezek, A. Malpica, M. Follen, and R. Richards-Kortum, "Microanatomical and biochemical origins of normal and precancerous cervical autofluorescence using laser-scanning fluorescence confocal microscopy," *Photochem. Photobiol.* **77**, 550–555 (2003).
18. R. Drezek, C. Brookner, I. Pavlova, I. Boiko, A. Malpica, R. Lotan, M. Follen, and R. Richards-Kortum, "Autofluorescence microscopy of fresh cervical-tissue sections reveals alterations in tissue biochemistry with dysplasia," *Photochem. Photobiol.* **73**, 636–641 (2001).
19. W. H. Westra and D. Sidransky, "Fluorescence visualization in oral neoplasia: shedding light on an old problem," *Clin. Cancer Res.* **12**, 6594–6597 (2006).
20. I. Georgakoudi, E. E. Sheets, M. G. Müller, V. Backman, C. P. Crum, K. Badizadegan, R. R. Dasari, and M. S. Feld, "Trinodal spectroscopy for the detection and characterization of cervical precancers *in vivo*," *Am. J. Obstet. Gynecol.* **186**, 374–382 (2002).
21. S. K. Chang, D. Arifler, R. Drezek, M. Follen, and R. Richards-Kortum, "Analytical model to describe fluorescence spectra of normal and preneoplastic epithelial tissue: comparison with Monte Carlo simulations and clinical measurements," *J. Biomed. Opt.* **9**, 511–522 (2004).
22. S. K. Chang, Y. N. Mirabal, E. N. Atkinson, D. Cox, A. Malpica, M. Follen, and R. Richards-Kortum, "Combined reflectance and fluorescence spectroscopy for *in vivo* detection of cervical pre-cancer," *J. Biomed. Opt.* **10**, 024031 (2005).

23. S. K. Chang, N. Marin, M. Follen, and R. Richards-Kortum, "Model-based analysis of clinical fluorescence spectroscopy for *in vivo* detection of cervical intraepithelial dysplasia," *J. Biomed. Opt.* **11**, 024008 (2006).
24. U. Utzinger and R. R. Richards-Kortum, "Fiber optic probes for biomedical optical spectroscopy," *J. Biomed. Opt.* **8**, 121–147 (2003).
25. M. C. Skala, G. M. Palmer, C. Zhu, Q. Liu, K. M. Vrotsos, C. L. Marshek-Stone, A. Gendron-Fitzpatrick, and N. Ramanujam, "Investigation of fiber-optic probe designs for optical spectroscopic diagnosis of epithelial pre-cancers," *Lasers Surg. Med.* **34**, 25–38 (2004).
26. Q. Liu and N. Ramanujam, "Experimental proof of the feasibility of using an angled fiber-optic probe for depth-sensitive fluorescence spectroscopy of turbid media," *Opt. Lett.* **29**, 2034–2036 (2004).
27. T. J. Pfefer, A. Agrawal, and R. A. Drezek, "Oblique-incidence illumination and collection for depth-selective fluorescence spectroscopy," *J. Biomed. Opt.* **10**, 044016 (2005).
28. T. J. Pfefer, L. S. Matchette, A. M. Ross, and M. N. Ediger, "Selective detection of fluorophore layers in turbid media: the role of fiber-optic probe design," *Opt. Lett.* **28**, 120–122 (2003).
29. A. Amelink and H. J. C. M. Sterenborg, "Measurement of the local optical properties of turbid media by differential path-length spectroscopy," *Appl. Opt.* **43**, 3048–3054 (2004).
30. R. A. Schwarz, D. Arifler, S. K. Chang, I. Pavlova, I. A. Hussain, V. Mack, B. Knight, R. Richards-Kortum, and A. M. Gillenwater, "Ball lens coupled fiber optic probe for depth-resolved spectroscopy of epithelial tissue," *Opt. Lett.* **30**, 1159–1161 (2005).
31. D. Arifler, R. A. Schwarz, S. K. Chang, and R. Richards-Kortum, "Reflectance spectroscopy for diagnosis of epithelial precancer: model-based analysis of fiber-optic probe designs to resolve spectral information from epithelium and stroma," *Appl. Opt.* **44**, 4291–4305 (2005).
32. A. L. Clark, A. Gillenwater, R. Alizadeh-Naderi, A. K. El-Naggar, and R. Richards-Kortum, "Detection and diagnosis of oral neoplasia with an optical coherence microscope," *J. Biomed. Opt.* **9**, 1271–1280 (2004).
33. K. Tae, A. K. El-Naggar, E. Yoo, L. Feng, J. J. Lee, W. K. Hong, W. N. Hittelman, and D. M. Shin, "Expression of vascular endothelial growth factor and microvessel density in head and neck tumorigenesis," *Clin. Cancer Res.* **6**, 2821–2828 (2000).